Electromagnetic Structure of the Neutron from Annihilation Reactions

Paul Larin [1,2,*], **Xiaorong Zhou** [3,4,*], **Jifeng Hu** [5,*], **Frank Maas** [1,2,6,*], **Rinaldo Ferroli Baldini** [7,*], **Haiming Hu** [8,*] and **Guangshun Huang** [3,4,*]

1 Helmholtz Institute Mainz, Staudinger Weg 18, D-55099 Mainz, Germany
2 Institute of Nuclear Physics, Johannes Gutenberg University, D-55128 Mainz, Germany
3 State Key Laboratory of Particle Detection and Electronics, Hefei 230026, China
4 Department of Modern Physics, University of Science and Technology of China, Hefei 230026, China
5 Guangdong Provincial Key Laboratory of Nuclear Science, Institute of Quantum Matter, South China Normal University, Guangzhou 510631, China
6 GSI Helmholtzzentrum für Schwerionenforschung GmbH, D-64291 Darmstadt, Germany
7 INFN Laboratori Nazionali di Frascati, I-00044 Frascati, Italy
8 Institute of High Energy Physics, Beijing 100049, China
* Correspondence: larinp@uni-mainz.de (P.L.); zxrong@ustc.edu.cn (X.Z.); hujf@scnu.edu.cn (J.H.); maas@him.uni-mainz.de (F.M.); Rinaldo.Baldini@lnf.infn.it (R.F.B.); huhm@ihep.ac.cn (H.H.); hgs@ustc.edu.cn (G.H.)

Abstract: The investigation of the fundamental properties of the nucleon is one of the most important topics in the modern hadron physics. Its internal structure and dynamics can be studied through the measurement of electromagnetic form factors which represent the simplest structure observables and serve as a test ground for our understanding of the strong interaction. Since the first attempt to measure the time-like form factors of the neutron, only four experiments published results on its structure from annihilation reactions. Due to the lack of statistics and experimental challenges, no individual determination of the form factors of the neutron has been possible so far. Modern developments of electron-positron colliders and the associated detectors allow to measure the effective FF of the neutron with the process $e^+e^- \rightarrow n\bar{n}$ with unprecedented precision at the BESIII experiment, which is based at the BEPCII collider in Beijing, China. In this report, we review the published results of the form factors on the neutron in the time-like regime, describe the experimental setup, and discuss their impact on our understanding of the strong interaction. Future works at BESIII will help to improve the precision of the neutron FFs and, combined with theoretical progress in this field, help to illuminate the properties of the neutron structure.

Keywords: form factors; neutron; nucleon structure; annihilation reactions; non-perturbative strong interaction

1. Introduction

The interaction of the constituents of the proton and the neutron are described by Quantum Chromodynamics (QCD). The internal structure and dynamics of the nucleon can be parametrized by the electromagnetic (EM) form factors (FFs) [1]. The internal complex structure emerges at low energy from strong interaction the and quark confinement. They are subject of ongoing investigation, both in theory and experiment. The FFs of the nucleon serve as a testing ground for the understanding of the non-perturbative regime of QCD. They parameterize the coupling between the virtual photon $\gamma^*(q^2)$ with the hadronic vector current J_{had}^μ, therefore describe the nucleon as it is seen by an EM probe at different four-momentum transfer squared q^2. A spin S = 1/2 particle like the nucleon is characterized by 2S + 1 = 2 FFs, the Dirac and Pauli FFs . More commonly used are their linear combinations-the electric $G_E(q^2) \equiv G_E$ and magnetic $G_M(q^2) \equiv G_M$ FFs [2]. FFs can be measured for negative and positive q^2 in the space-like (SL) and time-like (TL)

region, respectively, which are connected by analyticity. In the TL kinematical region, FFs are measured via annihilation involving an intermediate virtual photon with $q^2 > 4m_N^2$ (GeV/c)^2, where m_N is the nucleon mass. For example the annihilation of an electron e^- and a positron e^+ followed by the creation of a nucleon N and antinucleon $\overline{N}$ pair. Assuming one-photon exchange as the dominant process and the validity of the Born approximation, the corresponding differential cross section in the e^+e^- center-of-mass (CM) system can be written as

$$\frac{d\sigma_B^{e^+e^- \to N\overline{N}}}{d\Omega}(q^2, \theta) = \frac{\alpha_{em}^2 \beta C(q^2)}{4q^2}\left[\left(1 + \cos^2\theta\right)|G_M|^2 + \frac{1}{\tau}\sin^2\theta|G_E|^2\right], \qquad (1)$$

where θ is the angle between the beam direction and the nucleon in the CM system, α_{em} is the electromagnetic fine structure constant, $\beta = \sqrt{1 - 1/\tau}$ is the velocity of the final state nucleon, $C(q^2)$ is the Coulomb enhancement factor [3], and $\tau = q^2/4m_N^2$ a kinematical factor. In contrast to processes with charged particles in the final state, the Coulomb enhancement factor $C(q^2)$ is equal to unity for a process with a pure neutral final state like the signal reaction described in this review : $e^+e^- \to n\bar{n}$. The leading order Feynman diagram for such a process is shown in Figure 1.
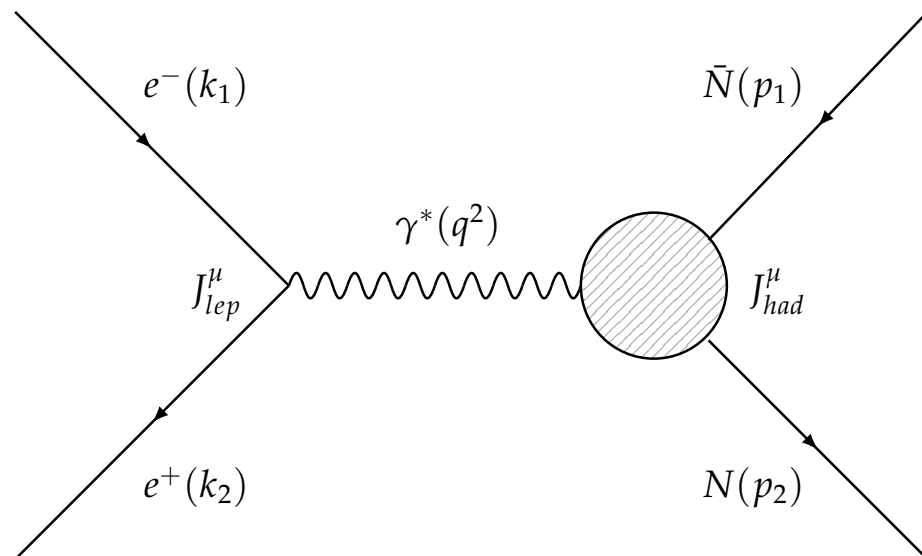
Figure 1. The lowest order Feynman diagram for the annihilation of an electron positron pair and the creation of a nucleon antinucleon pair $e^+e^- \to N\overline{N}$. k_1, k_2, p_1, and p_2 are the four-momenta of the incoming electron and positron and the outgoing four-momenta of the antinucleon and nucleon, respectively. $q^2 = (k_1 + k_2)^2 = (p_1 + p_2)^2 = s$ is the four-momentum transfer squared, J_{lep}^μ and J_{had}^μ are the leptonic and hadronic vector currents, $\gamma^*(q^2)$ is the virtual photon which transfers the four-momentum q^2 between the initial and final state of the reaction. The complex nucleon structure, encoded with the electromagnetc FFs, is sketched as the filled circle.

In the SL domain, with $q^2 < 0$ (GeV/c)^2, investigation of the nucleon structure can only be accessed by lepton-nucleon scattering and has been explored by many experiments since the pioneering work of Nobel laureate Hofstadter in 1958 [1]. Many experiments at SLAC, MIT-Bates, MAMI, JLab, and other electron accelerators contributed to our recent knowledge on the nucleon structure in the negative q^2 regime, where G_E and G_M are the Fourier transform of the distributions of the charge and magnetization of the nucleon. Detailed up-to-date summaries and reviews of experimental and theoretical achievements can be found in references [4–6].

In the TL region, the proton structure has been investigated in the past by many experiments, for example the PS170 experiment [7] at CERN, the BaBar experiment [8] at SLAC, and recently by the BESIII experiment [9–11] at IHEP, Beijing, among others. Its

effective FF $|G^p|$, the electric and magnetic FFs $|G^p_E|$ and $|G^p_M|$, as well as the ratio of the moduli of the FFs $|G^p_E|/|G^p_M|$ have been measured from lepton annihilation and antiproton annihilation. TL EM FFs are complex functions of four momentum transfer and can be acossiated with the time evolution of the electric charge and magnetization within the nucleon [12]. Reviews of the results can be found in [13,14]. The neutron on the other hand still remains a mystery due to experimental difficulty of detecting a neutral hadron and unavailibility of an anti-neutron beam. Only few experiments succeeded to investigate its structure and could only extract the so-called effective form factor due to limitations in statistics. The precise knowledge of the FFs of the neutron will not only help to provide a unified picture of the nucleon and solve open questions like the surprising results on the coupling strength between a virtual photon and the proton compared to the neutron [15], but also serve as input for nucleon models using dispersion relations [16] and vector meson dominance [17], to name only some.

In this article we will focus on experimental results on the TL EM FFs of the neutron.

2. Existing Measurements of the Time-like Form Factors of the Neutron

Experimental access to the neutron structure in the time-like region is very limited. Due to the lack of (anti-)neutron targets, the only process for the study of the TL FFs of the neutron is the reaction $e^+e^- \to n\bar{n}$. Different q^2-values can only be reached by scanning the beam energy. All available results have been obtained analysing this process. In principle, a second approach exists for such an investigation. The process $e^+e^- \to n\bar{n}\gamma_{ISR}$ can be studied using high luminosity data samples at fixed beam energy to analyze the Initial State Radiation (ISR) processes where the initial state photon carries away energy varying the q^2 at the annihilation vertex in a smooth manner over a wide range. Nevertheless, no successful attempt to use the latter exists up to date for the extraction of the neutron TL form factors.

When performing the analysis of an energy scan, the signal process $e^+e^- \to n\bar{n}$ is reconstructed from data samples taken at each beam energy value and the FFs are measured at different CM energies $\sqrt{s} = q^2 > 4m_n^2$. The moduli of the electric and magnetic FFs $|G^n_E(q^2)| \equiv |G^n_E|$ and $|G^n_M(q^2)| \equiv |G^n_M|$ can be determined from the angular distribution of the final state particles with respect to the polar angle θ in the e^+e^- CM frame and a precisely measured luminosity of the data. Until now, lack of statistics in the collected data prevented the individual determination of the FFs. Instead, all previous experiments measured the so-called effective form factor $|G^n|$ from the integrated Born cross section $\sigma_B^{n\bar{n}}$, under the hypothesis of equal electric and magnetic contributions $|G^n_E| = |G^n_M|$, which can be written as

$$\sigma_B^{n\bar{n}} = \frac{4\pi\alpha_{em}^2\beta}{3q^2}\left[|G^n_M|^2 + \frac{1}{2\tau}|G^n_E|^2\right], \qquad |G^n| = \sqrt{\frac{\sigma_B^{n\bar{n}}}{\frac{4\pi\alpha_{em}^2\beta}{3q^2}\left(1 + \frac{2m_n^2}{q^2}\right)}}. \qquad (2)$$

2.1. The DM2 Experiment

The first measurement of the neutron FFs from annihilation reactions has been published in 1988 by the DM2 experiment [18,19], located at the Orsay Storage Ring DCI [20] in France. The DM2 experiment measures e^+e^- collsions between $\sqrt{s} = 1.2 - 3.7$ GeV. It consists of a sub-system for charged particle detection made of two proportional chambers with anodes and cathodes read-out. It is complemented by a 13 layers thick drift chamber, a Cerenkov counter and a scintillation counter for the time of flight measurement. The whole setup is enclosed within a solenoid magnet providing a 0.5 T field. Outside of the magnet, 14 planes of wire tubes with longitudinal read-outs separated by lead sheets provide photon detection. A muon identifier is integrated in the flux return made of iron and concrete absorbers and wire tubes. More details on the detector setup can be found in [20].

One result for the neutron has been extracted from the Λ FF at $\sqrt{s} = 2.1$ GeV using the U-Spin symmetry [21]. This assumption is supposed to be valid at energies at which

one can neglect the strange quark mass. For this case, the electromagnetic interactions of hadrons with strangeness can be related to those without strangeness content, if they belong to the same SU(3) multiplet. The following relation has been used: $G_M^n \approx 2G_M^\Lambda$. A few events from $e^+e^- \to \Lambda\bar{\Lambda}$ have been reconstructed under the hypothesis $|G_E^n| = |G_M^n|$ leading to a magnetic form factor of the neutron of $|G_M^n| = 0.24^{+0.06}_{-0.04}$. Furthermore, the DM2 experiment reconstructed for the first time 2 candidate events using the energy scan channel $e^+e^- \to n\bar{n}$ at $\sqrt{s} = 2.4$ GeV, with one expected background event coming from cosmic rays. This measurement yielded a magnetic neutron FF of $|G_M^n| = 0.15 \pm 0.07$, again under the hypothesis $|G_E^n| = |G_M^n|$. Due to the assumption that the moduli of the electric and magnetic FFs are equal, these results are more closly identified with the effective FF than the magnetic one and are discussed as the former in this review. The results from the DM2 experiments are shown in Figure 2 as green filled squares.
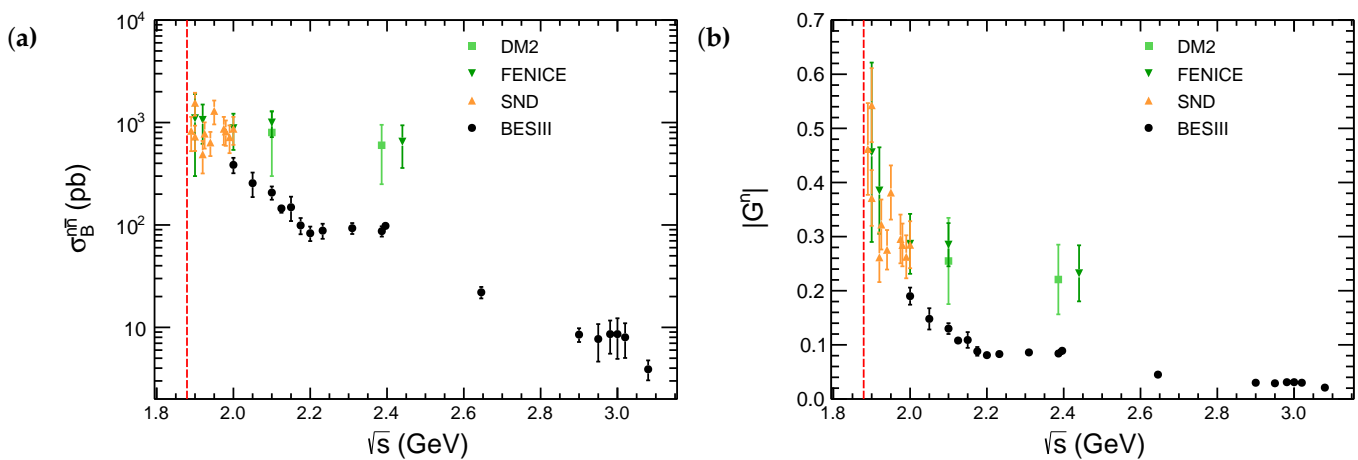

Figure 2. (**a**) Results for the Born cross section $\sigma_B^{n\bar{n}}$ with respect to the center-of-mass energy $\sqrt{s}$. (**b**) Results for the effective form factor $|G^n|$ with respect to the center-of-mass energy $\sqrt{s}$. The data shown as green squares is from the DM2 experiment [18,19], green downward triangles are results from the FENICE experiment [15,22], orange upward triangles show results from the SND experiment [23], and black dots represent the measurement from the BESIII experiment [24]. The total uncertainty of all data are determined as the quadratic sum of statistical and systematic errors, corresponding to a 68.3% confidence level of a normal distribution.

2.2. The FENICE Experiment

The first dedicated measurement on the magnetic neutron FF from annihilation was published in 1993 by the pioneering work of Antonelli A. et al. from the FENICE experiment [15,22] at the ADONE e^+e^- storage ring in Frascati, Italy. The five data sets range between $\sqrt{s} = 1.90$ and 2.44 GeV with a total integrated luminosity of 0.36 pb^{-1}. The main features of the non-magnetic detector comprise streamer tubes serving as a tracking system, a Time-of-Flight (ToF) and trigger system made of scintillator counters, and converters made of thin iron plates for the reconstruction of the star-shaped annihilation signature of the anti-neutron. No neutron signal was required to avoid its low detection efficiency. A detailed overview of the FENICE detector is given in reference [25].

The reconstruction of the signal process heavily relies on the ToF system, since the flight time of the anti-neutron is fixed by the two-particle final state kinematics and clearly differs in comparison to photons. Over all $\sqrt{s}$ a total sum of 74 signal events has been reconstructed. The integrated luminosity was measured with Bhabha scattering events ($e^+e^- \to e^+e^-$). While the integrated Born cross section $\sigma_B^{n\bar{n}}$ and the effective form factor $|G^n|$ have been derived, the determination of the separated FFs from angular distribution of the signal process was not possible due to the low statistics. Instead, the magnetic form factor has been calculated under two hypotheses: (i) $|G_E^n| = |G_M^n|$ and (ii) $|G_E^n| = 0$.

A visual inspection of the FENICE data angular distribution shows a preference for the second case (ii). The results for $|G_M^n|$ (under the hypothesis $|G_E^n| = 0$) from the FENICE experiment are shown in Figure 3a, the extracted effective FF is shown as green triangles in Figure 2.

(a)   **(b)**
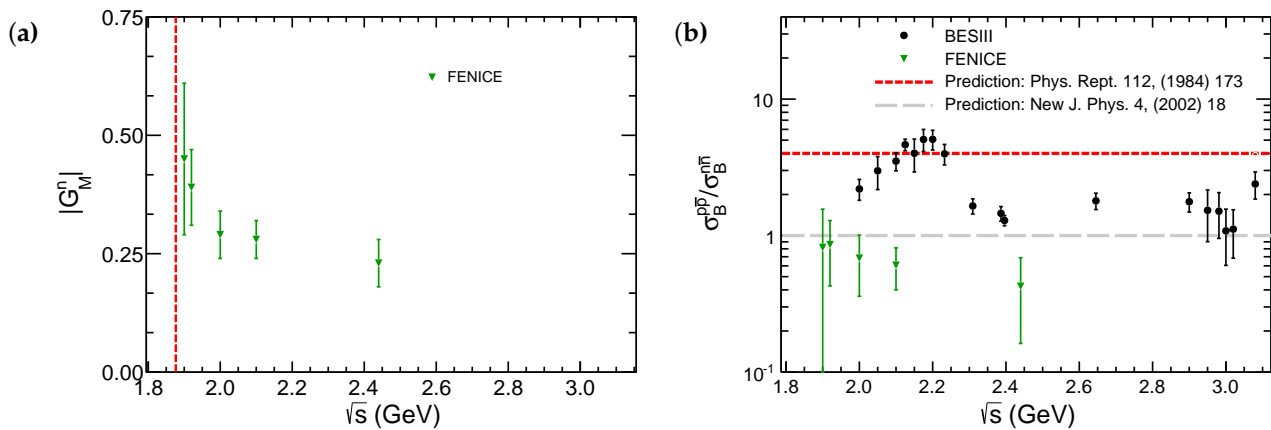
Figure 3. (**a**) Results for the magnetic form factor $|G_M^n|$ of the neutron from the FENICE experiment [21] under the hypothesis $|G_E^n| = 0$ with respect to the CM energy $\sqrt{s} = q$. The green downward triangles are experimental data. The red dashed line indicates the production threshold for the process $e^+e^- \to n\bar{n}$ at $2m_n$. (**b**) Results for the fraction of the Born cross sections $\sigma_B^{p\bar{p}}/\sigma_B^{n\bar{n}}$ neglecting the Coulomb enhancement factor. Green upward triangles are data from FENICE. The fine red dashed line and the coarse grey dashed line indicate the predicions from [26,27], respectively. The total uncertainty of all data are determined as the quadratic sum of statistical and systematic errors, corresponding to a 68.3% confidence level of a normal distribution.

2.3. The SND Experiment

The SND collaboration [28] at the VEPP-2000 e^+e^- collider in Novosibirsk, Russia, produced a set of high accuracy results on the TL neutron structure from the process $e^+e^- \to n\bar{n}$ with a total integrated luminosity of $\sim$10 pb^{-1}. Published in 2014 [23], results on $\sigma_B^{n\bar{n}}$ and $|G^n|$ are shown at 11 energy scan data points close to the production threshold between $\sqrt{s} = 1.88$ and 2.0 GeV. The data have been reconstructed with the non-magnetic SND detector. SND is a general purpose detector primarily designed to measure the hadronic cross section for an energy range between $\sqrt{s} = 0.3$ and 2.0 GeV. It is built from a tracking system consisting of a drift chamber and aerogel counters, Cherenkov counters and a muon detector. Its main component is a three-layer spherical NaI(Tl) electromagnetic calorimeter (EMC).

The reconstruction of the signal utilizes the characteristical unbalanced energy deposition from the neutron and anti-neutron in the EMC, respectively, and the non-zero event momentum. Cosmic rays background is significantly reduced with the muon detection system and the penetration depth within the EMC. Beam-related and physical background events are rejected with the EMC. The reconstructed events still contain a large fraction of cosmic ray background and other physical background like $e^+e^- \to p\bar{p}$. Physical background from the $p\bar{p}$ final state is considered with a dedicated measurement of such and taken into account when deriving the number of signal events, while other processes are considered within the systematics uncertainty. The precision of the results is given as $\sim$25% and 17% from statistics and systematic effects, respectively. The results for $\sigma_B^{n\bar{n}}$ are shown as orange triangles in Figure 2a. With the collected statistics, a meaningful determination of the separated FFs or their ratio $|G_E^n|/|G_M^n|$ was not possible, as stated by the authors.

2.4. The BESIII Experiment

The most recent measurement of the TL neutron FFs has been performed using the BESIII experiment [29] at the BEPCII e^+e^- collider located in Beijing, China. It utilizes the same process as all former experiments, but greatly exceeds the previously accumulated luminosity and energy range of the data available for analysis. A data set with a total integrated luminosity of 647.9 pb^{-1} at 18 energies between $\sqrt{s} = 2.0$ and 3.08 GeV was used to determine $\sigma_B^{n\bar{n}}$ and $|G^n|$. The results were published in 2021 [24] and represent the most precise and extensive measurement up to date. The signal process $e^+e^- \rightarrow n\bar{n}$ has been reconstructed with the multipurpose BESIII detector, which contains an inner tracking system and a solenoid magnet providing a 1 T field for the reconstruction of momenta and trajectories of charged particles, a ToF detector build from plastic scintillator bars to measure the flight time of charged particles from the e^+e^- interaction point, an EMC build from CsI(Tl) crystals for the measurement of energy deposition, and a layered muon detection system (MUC) for identification of muons and rejection of cosmic rays.

The signal reconstruction employs a unique way to classify pre-selected events with pure neutral final states. The detection of two stable neutral hadrons in the final state is extremely challenging. Events are sorted with respect to their interaction with the ToF and EMC. Three categories of events are defined, using the interaction of the neutron and anti-neutron, respectively, either in the ToF and/or the EMC. This approach guarantees the highest possible accumulation of reconstructed signal events and at the same time provides a cross-check of the individual selection strategies. Since the three classes of signal events are statistically independent, an error weighted combination greatly improves the statistical accuracy of the results. The data are not free of background, therefore the amount and distributions of the signal and background are investigated with dedicated Monte Carlo simulations that mimic the detector responses from the corresponding processes. Machine related and cosmic rays events, as well as background from the Toushek effect are studied from two data samples, which have been collected while the electron and positron beams have been tuned out of collision mode.

The precision of $\sigma_B^{n\bar{n}}$ is greatly improved when compared to previous measurements. The accuracy of $\sigma_B^{n\bar{n}}$ ranges between ~4–40% and ~6–16% from statistics and systematic effects, respectively. The results from BESIII on $\sigma_B^{n\bar{n}}$ and $|G^n|$ are shown as black dots in Figure 2.

3. Results

Figure 2a,b show the results on the Born cross section $\sigma_B^{n\bar{n}}$ and the effective form factor $|G^n|$, respectively. Old measurements from DM2 and FENICE are available at only few energies, while SND measured from the $n\bar{n}$ threshold to 2.0 GeV, and BESIII provides a wide coverage between $\sqrt{s} = 2.0$ and 3.08 GeV. The data from DM2 and FENICE show large uncertainties due to very low statistics. The results from SND-with an energy weighted average of 0.85 nb-are in agreement with the previous measurement from DM2 and FENICE. In later conference proceedings, i.e., in [30] (page 3, 2nd last paragraph), the authors from the SND publication note that the detection efficiency and the background study were found to contain problems and therefore the data will be re-analysed for a future publication. The shown results from [23] most likely underestimate various background sources and are considered as systematically overestimated. The results from BESIII, while the most precise, are systematically below all previous measurements, yet still within two standard deviations when the individual uncertainties are taken into account.

The only published data on the separated magnetic form factor of the neutron G_M^n for $q^2 > 0$ are from the FENICE experiment, as shown in Figure 3a. The extraction of these results was not assumption-free, but used the hypothesis of $G_E^n = 0$. This conclusion has been made by a visual inspection of the polar angle distribution from all collected signal events-in total 74-between $\sqrt{s} = 1.90$ and 2.44 GeV. In case of the proton it has been shown, that ratio of the moduli between the electric and magnetic form factors $|G_E^p|/|G_M^p|$ changes within this energy region [9], therefore-and in case that the neutron shows a similar behavior-an average over this energy region could hide a change of the polar angle distributions at different $\sqrt{s}$ values leading to a wrong assumption of $G_E^n = 0$.

The FENICE experiment measured additionally to the neutron channel the corresponding annihilation process with the proton in the final state $e^+e^- \to p\bar{p}$ with the same data set. Utilizing these results and neglecting the Coulomb enhancement factor in case of the proton, the ratio of the Born cross sections $\sigma_B^{p\bar{p}}/\sigma_B^{n\bar{n}}$ was calculated, as shown in Figure 3b. The surprising result indicates a stronger coupling of the virtual photon $\gamma^*(q^2)$ with the neutron, than with the proton, in contradiction to most theoretical predictions. As an example, the FENICE results on $\sigma_B^{p\bar{p}}/\sigma_B^{n\bar{n}}$ are compared with the naive quark model [26], shown as the red fine dashed line, and with a pQCD based model [27], indicated as the gray coarse dashed line. Also at the BESIII experiment the same data set was used to measure the processes $e^+e^- \to n\bar{n}$ and $e^+e^- \to p\bar{p}$ [9]. A test on the Born cross sections ratio $\sigma_B^{p\bar{p}}/\sigma_B^{n\bar{n}}$ and comparison to the surprising outcome from the FENICE experiment was made, as shown as black dots in Figure 3b. Similar to the approach at FENICE, the Coulomb enhancement factor in case of the proton is neglected. The BESIII results disagree with the older FENICE measurement, showing $\sigma_B^{p\bar{p}}/\sigma_B^{n\bar{n}} > 1$ as predicted from theory.

An interesting behavior in the effective form factor of the proton $|G^p|$ has been observed by the BaBar experiment [31] and confirmed by a recent BESIII measurement [10]. The proton data Figure 4a shows an oscillation around a modified dipole behavior, which is parametrized with $G_D(q^2)$

$$G_{osc}(q^2) = |G^p| - G_D, \quad G_D(q^2) = \frac{\mathcal{A}_n}{\left(1 - \frac{q^2}{0.71(\text{GeV}^2)}\right)^2 \left(1 + \frac{q^2}{m_a^2}\right)}. \tag{3}$$

with a normalization factor $\mathcal{A}_n$ and a pole parameter m_a^2. Authors in [32] proposed to employ an oscillation and an additional damping to reproduce this behaviour using the function

$$F_{osc} = A\exp(-Bp)\cos(Cp + D), \quad p \equiv \sqrt{E^2 - m_p^2}, \quad E \equiv \frac{q^2}{2m_p} - m_p \tag{4}$$

with a normalization A, an inverse oscillation damping parameter B, a momentum frequency C, a phase D and the proton mass and relative momentum m_p and p, respectively. BESIII found a similar effect in the neutron data, as shown as black dots in Figure 4b. Furthermore, the authors perform a simultaneous fit to the nucleon data using a common momentum frequency parameter C for both data sets. This approach can describe the proton and neutron data at the same time and hints that the observed oscillation could have a common reason. Further investigations of this effect could help to establish a global nucleon description.
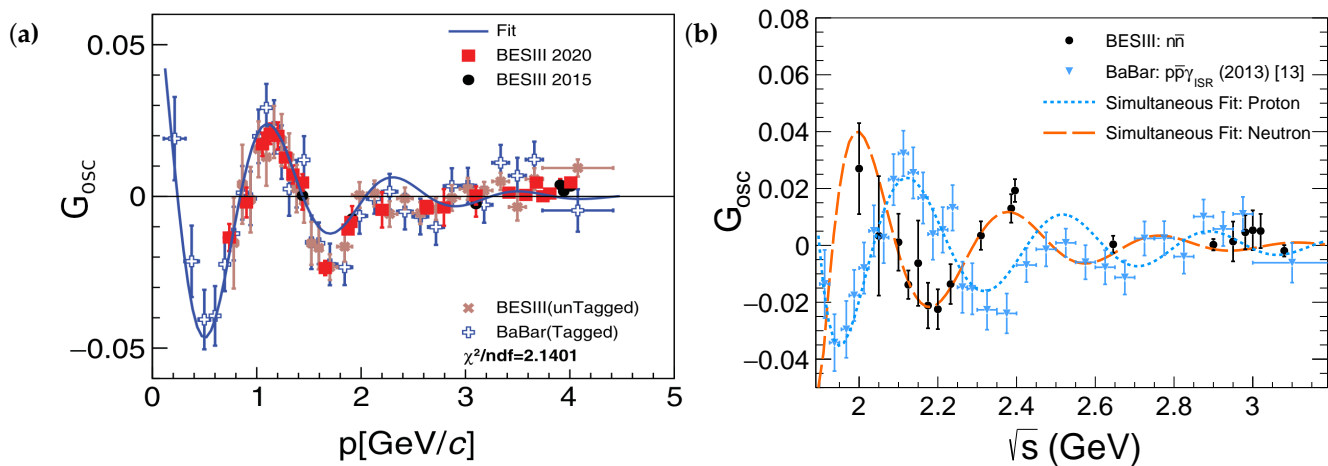
Figure 4. (**a**) Deviation of the effective form factor of the proton $|G^p|$ from the modified dipole law $G_D(q^2)$ with respect to the relative momentum of the proton, measured by the BaBar [31] and BESIII experiments [9,10]. The plot is taken from [33]. (**b**) Deviation of the nucleon effective form factor from the dipole law $G_D(q^2)$ with respect to the center-of-mass energy $\sqrt{s}$. Results for the neutron measured by the BESIII experiment [24] are shown as black circles, results for the proton from the BABAR experiment [31] are represented by the blue downward triangles. The coarse dashed orange line and fine dashed blue line show a simultaneous fit to the data. The plot is taken from [24]. The total uncertainty of all data in plot (**a**,**b**) is determined as the quadratic sum of statistical and systematic errors, corresponding to a 68.3% confidence level of a normal distribution.

4. Discussion and Prospects

With the accumulation of data and improved detection technology, impressive progress on the experimental determination of the em FFs of the neutron in TL domain has been made over the last thirty years. After the first attempt of the DM2 experiment, FENICE has successfully reconstructed signal events from the process $e^+e^- \to n\bar{n}$ at six energy points with $\sqrt{s}$ ranging from 1.90 to 2.44 GeV with a total of 74 ± 14 with an integrated luminosity of 0.36 pb^{-1}. The SND experiment recorded already hundreds of signal events with an integrated luminosity of 10 pb^{-1} from $n\bar{n}$ threshold up to 2 GeV. At BESIII, with an integrated luminosity of 647.9 pb^{-1}, the accumulated number of signal events of $e^+e^- \to n\bar{n}$ is around ∼2300 at 18 energy points covering a wide $\sqrt{s}$ range between 2.0 and 3.08 GeV.

The high precision measurement of the TL EM FFs of the neutron has been discussed by theory. Even before publication, the preprint version of the BESIII results [34] has been utilized together with not yet published data from SND and the high precission measurement of the TL EM FFs of the proton at BESIII [9] using a dispersion theoretical approach to describe the EM structure of the nucleon in a global view [35]. Together with experimental results from the SL region, the fitting approach based on dispersion theory can consistently describe the data for the proton and neutron structure for a wide positive and negative q^2, as shown in Figure 5. Additionally, the oscillating structures in the TL neutron and proton effective FFs are reproduced.

Three noteworthy results from the experimental measurements of the process $e^+e^- \to n\bar{n}$ are discussed in the following. The first one is an unexpectedly large Born cross section for the neutron channel $\sigma_B^{n\bar{n}}$ above $\sqrt{s} = 2$ GeV, observed by FENICE [15], and confirmed by SND [23]. The surprising large result has been drawing a lot of theoretical discussions since then. As in a perturbative QCD prediction from [26] the ratio for $e^+e^- \to p\bar{p}$ over $e^+e^- \to n\bar{n}$ should be proportional to the electric charges of the primary $q\bar{q}$ pairs, by following this approach one would expect for this fraction of cross sections a value of 4. While the most probable reason for the unexpectedly large cross section measured by FENICE and SND is a low statistics and analysis problems, as described before, several theoretical approaches have been given to resolve puzzle. A possible explanation is given in reference [33,36], where the reaction $e^+e^- \to N\bar{N}$ is interpreted as a two-step processes

via an intermediate coherent isovector state. In reference [36], the overall ratio of isospin-triplet and isospin singlet is given. In Ref. [33], a partial wave analysis is performed taking into account the two vector mesons $\omega(1930)$ and $\rho(2000)$. Using different states of the vector mesons, the model predicts various outcomes for the form factor ratio. The most recent experimental measurements from SND [30] and BESIII [24] seem to resolve this question with a significantly smaller $\sigma_B^{n\bar{n}}$ than $\sigma_B^{p\bar{p}}$ for $\sqrt{s}$ larger than 2 GeV. The dispersion theoretical fit from [35] predicts an effective FFs ratio $|G^p|/|G^n|$ larger than one, which is equivalent to $\sigma_B^{p\bar{p}}/\sigma_B^{n\bar{n}} > 1$, in agreement with the BESIII measurement [24] as well as with the theoretical predictions from the naive quark model [26]. However, more results are needed, especially for separated FFs $|G_E|$ and $|G_M|$, to confirm the experimental situation and to obtain enough input for precise theoretical descriptions to finally resolve this puzzle.
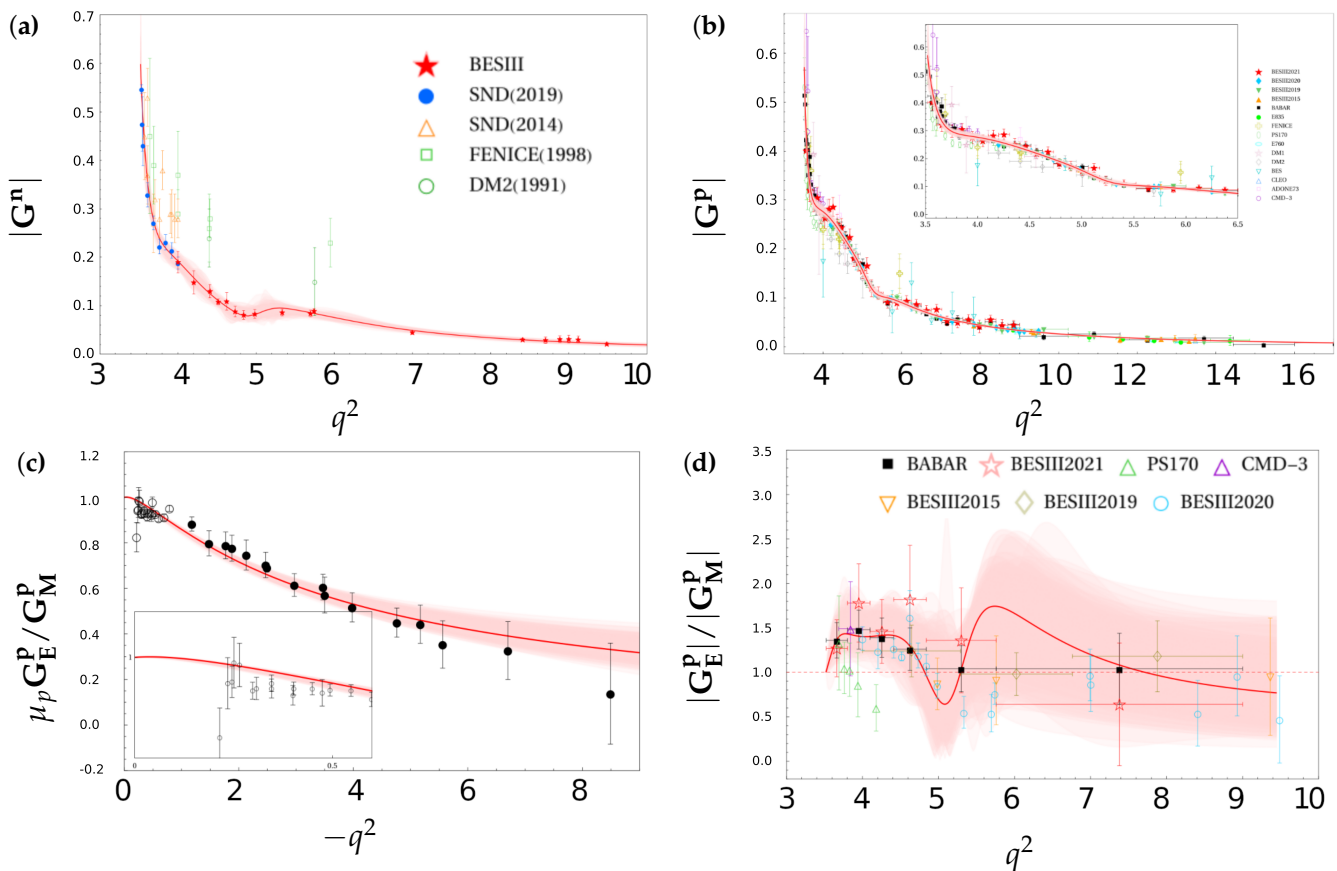
Figure 5. Global fit to the SL and TL data for the em FFs of the nucleon. (**a**) Effective FF of the neutron $|G^n|$, (**b**) effective FF of the proton $|G^p|$, (**c**) the SL em FFs ratio of the proton $\mu_p G_E^p/G_M^p$, and (**d**) the TL EM FFs ratio of the proton $|G_E^p|/|G_M^p|$ with respect to q^2. The filled data are used for the fit, while the open data are shown only for comparison. A full list of the references for the used experimental data, as well as the details of the fit can be found in the corresponding reference. The plots are taken from [35].

The second surprising result is the non-zero cross section of $e^+e^- \rightarrow n\bar{n}$ near threshold at $\sqrt{s} = 1.9$ GeV observed by SND. It is unexpected, since according to theoretical predictions the production cross section for neutral baryon pairs at threshold should be zero due to phase space limitation. Unlike the situation for neutral baryons, the production cross section of charged baryon pairs at threshold can be non-zero with a cancelation of the phase space from a Coulomb enhencement factor. The plateau distribution is also considered as an abnormal threshold effect. The physics scenarios under the threshold effects can be interpreted from the contribution of a meson-resonance [33,37], a baryon-antibaryon bound state near threshold [38], or more corrections on the pQCD prediction [39] etc.

The third surprising result comes from the most precise measurements by BESIII, where an oscillation behavior is observed for the neutron effective FF $|G^n|$ after subtraction of the well-established dipole function, denoted as residue FF. Following a kinematic approach it is found that the damping factors of the oscillation are the same for proton and neutron while their phases are almost orthogonal. This result implies that there are some intrinsic dynamics not yet understood that are responsible for these unexpected oscillations. Various theoretical interpretations have been performed to reveal the origin the oscillation feature [35,40,41]. Possible explanations are interference effects from final state re-scattering, or contribution due to a resonant structure. A recent paper [37] discussed the residue FF in terms of contributions from the finite width of vector mesons, i.e., $\rho(1900)$, $\phi(2170)$ and $X(2400)$, and can describe BESIII data well. Figure 6 show the fit of Breit-Wigner distribution and Gaussian function, as well as the original damping oscillation function for the residue FF lineshape.
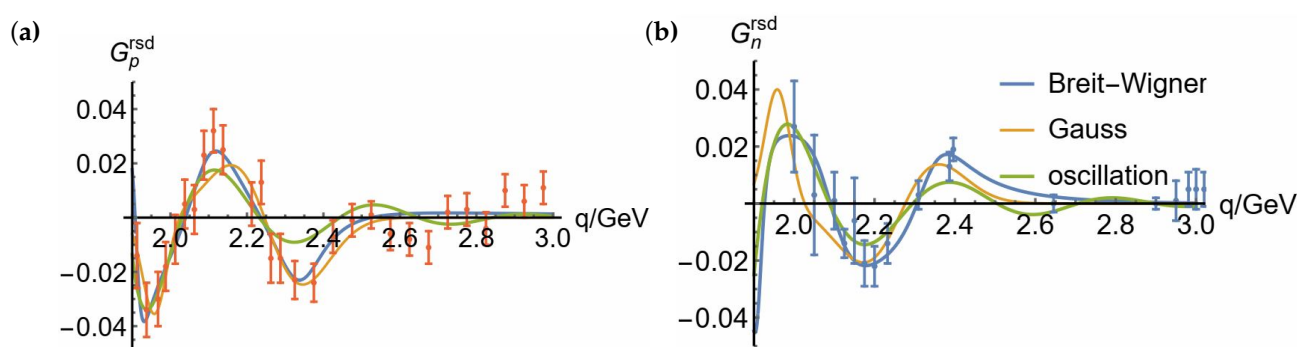
Figure 6. Fit with Breit-Wigner distribution and Gaussian distribution to the three local structures in the residue FFs of the (**a**) proton and (**b**) neutron. The fitting results include the original damping oscillation function for the residue FF lineshape. The plots are taken from [37].

The separated em FFs and their ratio $|G_E^n|/|G_M^n|$ can only be obtained by analyzing the angular distribution of the final state neutrons, thus more statistics are needed to disentangle the electromagnetic FFs. Further analysis of the BESIII data used for the study in [24] is foreseen to disentangle the electromagnetic FFs for the first time without employing assumptions, as before by the FENICE experiment. Moreover, the proposed Super tau-charm factory projects in China [42] and Russia [43], with an integrated luminosity two magnitudes higher than that of BEPCII, show great potential to reach high precision in the measurement of the cross section for $e^+e^- \rightarrow n\bar{n}$ and the $|G_E^n|/|G_M^n|$ ratio.

Author Contributions: Conceptualization, P.L., X.Z., J.H., F.M., R.F.B., H.H. and G.H.; Formal analysis, P.L., X.Z. and J.H.; Funding acquisition, F.M. and H.H. and G.H.; Investigation, P.L., X.Z. and J.H., F.M., R.F.B., H.H. and G.H.; Methodology, P.L., X.Z. and J.H.; Software, P.L., X.Z. and J.H.; Supervision, F.M., R.F.B., H.H. and G.H.; Validation, all authors; Writing—original draft, P.L. and X.Z.;Writing—review & editing, P.L., X.Z., F.M. and G.H. All authors have read and agreed to the published version of the manuscript.

Institutional Review Board Statement: Not applicable.

Informed Consent Statement: Not applicable.

References

1. Yearian, M.R.; Hofstadter, R. Magnetic Form Factor of the Neutron. *Phys. Rev.* **1958**, *110*, 52. [CrossRef]
2. Hand, L.N.; Miller, D.G.; Wilson, R. Electric and Magnetic Formfactor of the Nucleon. *Rev. Mod. Phys.* **1963**, *35*, 335. [CrossRef]
3. Arbuzov, A.B.; Kopylova, T.V. On relativization of the Sommerfeld-Gamow-Sakharov factor. *J. High Energy Phys.* **2012**, *4*, 9. [CrossRef]
4. Perdrisat, C.F.; Punjabi, V.; Vanderhaeghen, M. Nucleon Electromagnetic Form Factors. *Prog. Part. Nucl. Phys.* **2007**, *59* 694–764. [CrossRef]
5. Arrington, J.; De Jager, K.; Perdrisat, C.F. Nucleon Form Factors: A Jefferson Lab Perspective. *J. Phys. Conf. Ser.* **2011**, *299*, 012002. [CrossRef]
6. Puckett, A.J.; Brash, E.J.; Jones, M.J.; Luo, W.; Meziane, M.; Pentchev, L.; Perdrisat, C.F.; Punjabi, V.; Wesselmann, F.R.; Afanasev, A.; et al. Polarization Transfer Observables in Elastic Electron Proton Scattering at $Q^2 = 2.5, 5.2, 6.8,$ and $8.5 \, \mathrm{GeV}^2$. *Phys. Rev. C* **2017**, *96*, 055203, Erratum in *Phys. Rev. C* **2018**, *98*, 019907. [CrossRef]
7. Bardin, G.; Burgun, G.; Calabrese, R.; Capon, G.; Carlin, R.; Dalpiaz, P.; Dalpiaz, P.F.; Derré, J.; Dosselli, U.; Duclos, J.; et al. Determination of the electric and magnetic form-factors of the proton in the timelike region. *Nucl. Phys. B* **1994**, *411*, 3–32. [CrossRef]
8. Aubert, B.; Barate, R.; Boutigny, D.; Couderc, F.; Karyotakis, Y.; Lees, J.P.; Poireau, V.; Tisserand, V.; Zghiche, A.; Grauges, E.; et al. A Study of $e^+e^- \to p\bar{p}$ using initial state radiation with BABAR. *Phys. Rev. D* **2006**, *73*, 012005. [CrossRef]
9. Ablikim, M.; Achasov, M.N.; Adlarson, P.; Ahmed, S.; Albrecht, M.; Alekseev, M.; Amoroso, A.; An, F.F.; An, Q.; Bai, Y.; et al. BESIII Collaboration; Measurement of proton electromagnetic form factors in $e^+e^- \to p\bar{p}$ in the energy region 2.00–3.08 GeV. *Phys. Rev. Lett.* **2020**, *124*, 042001. [CrossRef] [PubMed]
10. Ablikim, M.; Achasov, M.N.; Adlarson, P.; Ahmed, S.; Albrecht, M.; Alexeev, M.G.; Amoroso, A.; An, F.; An, Q.; Bai, Y.; et al.; BESIII Collaboration; Study of the process $e^+e^- \to p\bar{p}$ via initial state radiation at BESIII. *Phys. Rev. D* **2019**, *99*, 092002. [CrossRef]
11. Huang, G.S.; Baldini Ferroli, R. Probing the internal structure of baryons. *Natl. Sci. Rev.* **2021**, *8*, nwab187. [CrossRef] [PubMed]
12. Maggiora, M.; BESIII Collaboration. New results on nucleon/baryon time-like form factors. *AIP Conf. Proc.* **2020**, *2249*, 030019.
13. Xia, L.; Rosner, C.; Wang, Y.; Zhou, X.; Maas, F.E.; Ferroli, R.B.; Hu, H.; Huang, G. Proton Electromagnetic Form Factors in the Time-like Region through the Scan Technique. *Symmetry* **2022**, *14*, 231. [CrossRef]
14. Lin, D.; Dbeyssi, A.; Maas, F. Time-like Proton Form Factors with Initial State Radiation Technique. *Symmetry* **2022**, *14*, 91. [CrossRef]
15. Antonelli, A.; Baldini, R.; Benasi, P.; Bertani, M.; Biagini, M.E.; Bidoli, V.; Bini, C.; Bressani, T.; Calabrese, R.; Cardarelli, R.; et al. FENICE Collaboration. The first measurement of the neutron electromagnetic form-factors in the timelike region. *Nucl. Phys. B* **1998**, *517*, 3–35. [CrossRef]
16. Hammer, H.W. Nucleon form-factors in the space-like and time-like regions. *Electron. Conf. Proc. C* **2001**, *C010430*, W08.
17. Bijker, R.; Iachello, F. Reanalysis of the nucleon spacelike and timelike electromagnetic form factors in a two-component model. *Phys. Rev. C* **2004**, *69*, 068201. [CrossRef]
18. Castro, A.; DM2 Collaboration. *The pi, K, Proton Electromagnetic Form-Factor and New Related DM2 Results*; Internal Note LAL-88-58; International Atomic Energy Agency (IAEA): Vienna, Austria, 1988.
19. Biagini, M.E.; Pasqualucci, E.; Rotondo, A. U spin considerations to guess the unknown timelike neutron form-factors. *Z. Phys. C* **1991**, *52*, 631–634. [CrossRef]
20. Augustin, J.E.; Bussetto, G.; Capon, G.; Cosme, G.; Dudelzak, B.; Eschstruth, P.; Fulda, F.; Grelaud, B.; Grosdidier, G.; Jean-Marie, B.; et al. Dm2: A Magnetic Detector for the Orsay Storage Ring DCI. *Phys. Scr.* **1981**, *23*, 623–633. [CrossRef]
21. Coleman, S.R.; Glashow, S.L. Electrodynamic properties of baryons in the unitary symmetry scheme. *Phys. Rev. Lett.* **1961**, *6*, 423. [CrossRef]
22. Antonelli, A.; Baldini, F.R.; Bertani, M.; Biagini, M.E.; Bidoli, V.; Bini, C.; Bressani, T.; Calabrese, R.; Cardarelli, R.; Carlin, R.; et al. First measurement of the neutron electromagnetic form-factor in the timelike region. *Phys. Lett. B* **1993**, *313*, 283–287. [CrossRef]
23. Achasov, M.N.; Barnyakov, A.Y.; Beloborodov, K.I.; Berdyugin, A.V.; Berkaev, D.E.; Bogdanchikov, A.G.; Botov, A.A.; Dimova, T.V.; Druzhinin, V.P.; Golubev, V.B.; et al. Study of the process $e^+e^- \to n\bar{n}$ at the VEPP-2000 e^+e^- collider with the SND detector. *Phys. Rev. D* **2014**, *90*, 112007. [CrossRef]
24. Ablikim, M.; Achasov, M.P.; Adlarson, S.; Ahmed, M.; Albrecht, M.; Aliberti, A.; Amoroso, A.; An, Q.; Lavania, A.; Bai, X.H.; et al. The BESIII Collaboration. Oscillating features in the electromagnetic structure of the neutron. *Nat. Phys.* **2021**, *17*, 1200–1204.
25. Antonelli, A.; Baldini, R.; Balla, A.; Becciani, C.; Bertani, M.; Biagini, M.E.; Bini, C.; Bidoli, V.; Voci, C.; FENICE Collaboration; et al. The FENICE detector at the e^+e^- collider ADONE. *Nucl. Instrum. Methods Phys. Res. Sect. A* **1993**, *337*, 34–43. [CrossRef]
26. Chernyak, V.L.; Zhitnitsky, A.R. Asymptotic behavior of exclusive processes in QCD. *Phys. Rept.* **1984**, *112*, 173–318. [CrossRef]

27. Pacetti, S.; Baldini, F.R.; Tomasi-Gustafsson, E. Proton electromagnetic form factors: Basic notions, present achievements and future perspectives. *Phys. Rep.* **2015**, *550–551*, 1–103. [CrossRef]

28. Achasov, M.N.; Berkaev, D.E.; Bogdanchikov, A.G.; Bukin, D.A.; Koop, I.A.; Korol, A.A.; Koshuba, S.V.; Kovrizhin, D.P.; Otboev, A.V.; Perevedentsev, E.A.; et al. First experience with SND calorimeter at VEPP-2000 collider. *Nucl. Instrum. Meth. A* **2009**, *598*, 31–32. [CrossRef]

29. Yuan, C.Z.; Olsen, S.L. The BESIII physics programme. *Nat. Rev. Phys.* **2019**, *1*, 480–494. [CrossRef]

30. Druzhinin, V.P.; Serednyakov, S.I. Measurement of the $e^+e^- \to n\bar{n}$ cross section with the SND detector at the VEPP-2000 collider. *EPJ Web Conf.* **2019**, *212*, 07007. [CrossRef]

31. Lees, J.P.; BABAR Collaboration. Study of $e^+e^- \to p\bar{p}$ via initial-state radiation at BABAR. *Phys. Rev. D* **2013**, *87*, 092005. [CrossRef]

32. Bianconi, A.; Tomasi-Gustafsson, E. Periodic interference structures in the timelike proton form factor. *Phys. Rev. Lett.* **2015**, *114*, 232301. [CrossRef]

33. Yan, Y.; Khosonthongkee, K.; Kobdaj, C.; Suebka, P. $e^+e^- \to$anti-N N at Threshold and Proton Form Factor. *J. Phys. G* **2010**, *37*, 075007. [CrossRef]

34. Ablikim, M. et al. BESIII Collaboration; et al. New Features in the Electromagnetic Structure of the Neutron. *arXiv* **2021**, arXiv:2103.12486.

35. Lin, Y.H.; Hammer, H.W.; Meißner, U.G. New insights into the nucleon's electromagnetic structure. *arXiv* **2021**, arXiv:2109.12961.

36. Ellis, J.R.; Karliner, M. On electron positron annihilation into nucleon anti-nucleon pairs. *New J. Phys.* **2002**, *4*, 18. [CrossRef]

37. Cao, X.; Dai, J.P. Timelike nucleon electromagnetic form factors: All about interference of isospin amplitudes. *arXiv* **2021**, arXiv:2109.15132.

38. Cotugno, G.; Faccini, R.; Polosa, A.D.; Sabelli, C. Charmed Baryonium. *Phys. Rev. Lett.* **2010**, *104*, 132005. [CrossRef] [PubMed]

39. Baldini, F.R.; Pacetti, S.; Zallo, A. Point-like Baryons? *arXiv* **2008**, arXiv:0812.3283.

40. Tomasi-Gustafsson, E.; Bianconi, A.; Pacetti, A. New fit of timelike proton electromagnetic formfactors from e^+e^- colliders. *Phys. Rev. C* **2021**, *103*, 035203. [CrossRef]

41. Lorenz, I.T.; Hammer, H.W.; Meißner, U.G. New structures in the proton-antiproton system. *Phys. Rev. D* **2015**, *92*, 034018. [CrossRef]

42. Shi, X.D.; Zhou, X.R.; Qin, X.S.; Peng, H.P. A fast simulation package for STCF detector. *J. Instrum.* **2021**, *16*, P03029. [CrossRef]

43. Eidelman, S. Project of the Super-tau-charm Factory in Novosibirsk. *Nucl. Part. Phys. Proc.* **2015**, *260*, 138–241. [CrossRef]